J Solid State Electrochem (2016) 20:957–967
DOI 10.1007/s10008-015-2983-8

ORIGINAL PAPER

Electrochemical gating of single osmium molecules tethered to Au surfaces

Santiago Herrera[1] · **Catherine Adam**[1] · **Alejandra Ricci**[1,2] · **Ernesto J. Calvo**[1]

Received: 18 May 2015 / Revised: 16 July 2015 / Accepted: 20 July 2015 / Published online: 8 August 2015

Abstract The electrochemical study of electron transport between Au electrodes and the redox molecule $Os[(bpy)_2(PyCH_2NH_2CO-]ClO_4$ tethered to molecular linkers of different length (1.3 to 2.9 nm) to Au surfaces has shown an exponential decay of the rate constant k_{ET}^0 with a slope $\beta = 0.53$ consistent with through bond tunneling to the redox center. Electrochemical gating of single osmium molecules in an asymmetric tunneling nano-gap between a Au(111) substrate electrode modified with the redox molecules and a Pt-Ir tip of a scanning tunneling microscope was achieved by independent control of the reference electrode potential in the electrolyte, $E_{ref} - E_s$, and the tip-substrate bias potential, E_{bias}. Enhanced tunneling current at the osmium complex redox potential was observed as compared to the off resonance set point tunneling current with a linear dependence of the overpotential at maximum current vs. the E_{bias}. This corresponds to a sequential two-step electron transfer with partial vibration relaxation from the substrate Au(111) to the redox molecule in the nano-gap and from this redox state to the Pt-Ir tip according to the model of Kuznetsov and Ulstrup (J Phys Chem A 104: 11531, 2000). Comparison of short and long linkers of the osmium complex has shown the same two-step ET (electron transfer) behavior due to the long time scale in the complete reduction-oxidation cycle in the electrochemical tunneling spectroscopy (EC-STS) experiment as compared to the time constants for electron transfer for all linker distances, k_{ET}^0.

Keywords Self-assembled monolayer · Osmium complex · Electronic transfer · Electrochemical scanning tunneling spectroscopy-gating

Introduction

It seems most appropriate for the 65th birthday celebration of Professor Jose (Pepe) Zagal to report on some aspects of the electron transfer (ET) in electrochemical experiments given his contributions to the field, in particular in free energy relations in electrocatalysis [1, 2].

A remarkable progress in the measurement of the electrical and electrochemical behavior of single molecules has been reached in recent years [3]. The first proposal for a molecular rectifier or molecular transistor was in 1974 by M. Ratner and A. Aviram [4]. Subsequently, Chidsey [5] pioneered the work on electron transfer to redox self-assembled monolayers (SAMs) with terminal ferrocene redox groups and verified the validity of Marcus theory [6–10] of electron transfer at electrodes. N. Tao [11] introduced electrochemical STM of adsorbed iron protoporphyrin IX film on highly oriented pyrolytic graphite (HOPG) by changing the redox states Fe(II) and Fe(III) with the modulation of the substrate electrode potential with respect to the reference electrode while measuring STM in constant current mode [11]. Tao and Schmickler [12] further described these experiments with a Gaussian density of redox states and measured the inverted region of the electron transfer reaction of Fe(III)-protoporphyrin IX film.

In situ electrochemical metal/molecule/metal scanning tunneling spectroscopy (EC-STS) of redox active molecules has been reported by the groups of Ulstrup [13–17] (Os and

This work is dedicated to Prof. Jose H. Zagal on the occasion of his 65th birthday.

✉ Ernesto J. Calvo
calvo@qi.fcen.uba.ar

[1] INQUIMAE. Facultad de Ciencias Exactas y Naturales, Universidad de Buenos Aires, Pabellón 2, Ciudad Universitaria, AR-1419 Buenos Aires, Argentina

[2] Present address: Aluar, Puerto Madryn, Chubut U1200IA, Argentina

Co complexes), Wandlowski [18–21] (ferrocene, viologen), and Amatore [22] (ferrocene and Os complexes). In these experiments, a redox molecule in the nano-gap between the substrate and STM tip with energy levels accessible within the potential window explored provide electron transfer channels with tunneling current enhancement and diode-like current rectification. These molecules are attached to Au or Pt surfaces at the end of long-insulating N or S linkers so that the redox system is electrostatically decoupled from the electrode.

Our group has contributed with similar studies of Au-C and Au-S short-tethered Os bipyridine-pyridine chloride complex in the STM "tunneling gap" configuration with similar sequential two-step ET mechanism between the molecule and the tip and substrate metal contacts with partial vibration relaxation [23]. The $Os[(bpy)_2\ (PyCH_2NH_2CO\text{-}]ClO_4$ attached to Au electrodes by self-assembling mercapto alkanoic or mercaptobenzoic acids with post-functionalization via amide formation with primary amines in the metal complex has been reported by Ricci et al. [23–28].

In this communication, we present the systematic study of electron transfer kinetics at different length between the electrode and the redox probe by using different linkers with increasing number CH_2 units and benzene ring linkers. The choice of an outer sphere stable osmium bipyridine-pyridine complex resulted from previous electrochemical and STM studies so that the same electron acceptor/donor molecule has been used for different tether distances. We have thus extended the electrochemical and gated EC-STS tunneling current studies to longer mercaptoalkanoic acid tethers of the same $Os[(bpy)_2(PyCH_2NH_2CO\text{-}]ClO_4$ redox active molecule with larger electrostatic decoupling of the redox system and the electrode and decreasing ET rate by modulating the tunneling probability with distance.

ET in electrochemical experiments

In the electrochemical experiment between an electron donor (acceptor) electronic state at the electrode to an acceptor (donor) molecular level the electron (hole) is localized in the molecule [22]. A pseudo-capacitive behavior is observed with a current maximum at the formal potential of the redox molecule in the local environment at the surface in contact with the electrolyte [29]. The pseudo-capacitive current at the electrode with the redox molecule total concentration Γ_0, which will be one half oxidized one half reduced at the formal redox potential $E^{0\prime}$ and totally reduced or totally oxidized at the extreme potentials depends on the electrode potential as follows:

$$C_{\text{redox}} = \frac{i}{\nu} = \frac{A\Gamma_0 \exp\left(\frac{F}{RT}\left(E - E^{0\prime}\right)\right)}{\left[1 + \exp\left(\frac{F}{RT}\left(E - E^{0\prime}\right)\right)\right]^2} \quad (1)$$

With F as the Faraday constant, R the universal gas constant, T the absolute temperature, and ν the electrode potential scan rate. The peak current at $E = E^{0\prime}$ is given by

$$i_p = \frac{n^2 F^2}{4RT} \nu A \Gamma_0 \quad (2)$$

While the rate of electron transfer is given by the Gerischer [30]-Marcus-Levich-Dogonadze-Kuznetzov expression [31–33]

$$k_{ET}^0 = Z_{el}\kappa_{el}\exp[\beta(r - r_0)]\exp\left[\frac{\left(\lambda + F\left(E - E^0\right)\right)^2}{4\lambda k_B T}\right] \quad (3)$$

Where $Z_{\text{el}} \sim 10^4\ \text{cm}^2\ \text{s}^{-1}$, κ_{el} the transmission coefficient, $\beta \sim 10\ \text{nm}^{-1}$ [34], $d = r - r_0$ the tunneling distance between electrode and tethered redox molecule, λ the reorganization energy of the molecule internal modes and surrounding solvent vibrations, and k_{B} the Boltzmann constant.

Chidsey verified the validity Eq. (3) in 1991 using self-assembled blocking alkanethiol monolayers carrying a terminal ferrocene redox group and proved the validity of Marcus theory of electron transfer at electrodes by removing diffusion limitations [5].The exponential dependence decay of electrode current with distance has been verified by a large number of experimental evidence [34].

Albrecht et al. [13, 15–17] have reported electrochemical STM studies of several osmium complexes $[Os(byp)_2(p2p)]^{3+/2+}$ ($E^{0\prime}$ = 0.62 V) and $[Os(byp)_2(p0p)]^{2+/+}$ ($E^{0\prime}$ = 0.23 V), where byp = 2,2′-bipyridine, p2p = 1,2bis(4-pyridyl)ethane and p0p = 4,4′-bipyridine. These redox molecules exhibit very fast electron transfer kinetics, with $k_{ET} > 10^6\ s^{-1}$ *and feature electrochemical STM enhancement with a maximum above the off resonance tunneling current and a peak potential that depends on the electrochemical overpotential,* $\eta = E_S - E^{0\prime}$ *and tip-substrate bias,* E_{bias}*, with a width of 200–300 mV from confined space in the nano-gap between substrate and tip. Also, a systematic linear variation of peak potential in the tunneling current over potential curve with* E_{bias} *has been observed [35]. This experimental evidence corresponds to the Kuznetsov and Ulstrup two sequential electrochemical ET model with strong electronic coupling between Os complexes and substrate and tip electrodes [36]. Wandlowski also reported a two-step mechanism for the redox-active asymmetric tunneling junction formed between a Au STM tip and a Au(111) surface modified with 6-thiohexanoyl ferrocene in an electrochemical environment [20].*

In molecular conductance experiments, the redox molecule is a bridge between acceptor and donor electrodes and the charge simply passes through the structure by tunneling assisted by quantum coupling between the redox molecule and the electrodes, in the present case the substrate and the STM tip [22].

For the conductance experiments, there are several possibilities, i.e., in direct tunneling (off resonance), current flows between the STM tip and the electrode substrate independently of the redox chemistry of the bridge molecule, i.e., totally oxidized or totally reduced osmium complex in the present case. The energy levels of the Os(II) and Os(III) molecules fluctuate with respect to their equilibrium positions due to fluctuations of solvent molecules around the redox complex to a maximum of the reorganization energy, λ. When the Fermi level of one of the electrodes (substrate or tip) at tunneling distance in the nano-gap gets close to the Os(III) (unoccupied) or Os(II) (occupied) during the solvent fluctuation, the first ET event takes place within k_BT interval of the Fermi level (Fig. 1).

Then the electron (hole) occupancy in the redox molecular bridge in the STM nano-junction may relax by immediate transference to the second electrode without vibration relaxation of the Os molecule and solvation shell (resonance tunneling). If the molecule has enough time to relax vibrationally under weak electron coupling of the electronic states, the second ET takes place from the totally relaxed redox molecule (hopping mechanism). However, a larger tunneling current enhancement has been observed under strong electronic coupling between the redox molecule and the electrodes with many electrons being transferred in a single molecular reduction-oxidation cycle [36]. A two-step ET with partial vibration relaxation model has been described in this later case by Kuznezov and Ulstrup as depicted in Fig. 1 [15, 36]. In the adiabatic limit, the dependence of the tunneling current with the bias potential and the sample potential is expressed by the equation [37]

$$\frac{1}{I} = \frac{1}{2ek_{\mathrm{ET},1}} + \frac{1}{2ek_{\mathrm{ET},2}} \tag{4}$$

Where $k_{\mathrm{ET},1}$ and $k_{\mathrm{ET},2}$ are the respective rate constants for the substrate to molecule and molecule to tip ET processes [14]

$$k_{\mathrm{ET},1} = \frac{\omega_{\mathrm{eff}}}{2\pi}\exp\left[-\frac{(\lambda + e\xi\eta + e\gamma E_{\mathrm{bias}})^2}{4\lambda k_B T}\right] \tag{5}$$

$$k_{\mathrm{ET},2} = \frac{\omega_{\mathrm{eff}}}{2\pi}\exp\left[-\frac{(\lambda - eE_{\mathrm{bias}} + e\xi\eta - e\gamma E_{\mathrm{bias}})^2}{4\lambda k_B T}\right] \tag{6}$$

Where e is the elementary charge, κ is the electronic transmission coefficient, ρ is the density of electronic states in the metal near the Fermi level, ω_{eff} is the characteristic nuclear vibration frequency, λ is the reorganization free energy, η is the overpotential ($E_s - E^{0\prime}$), k_B is the Boltzmann constant, T the temperature, e the electron charge; $0.5 < \xi < 1$ and $0 \le \gamma \le 1$ are parameters describing the drops of the substrate potential and bias voltage at the redox center in the tunneling gap, respectively. In Fig. 1, the subscripts 1 and 2 refer to the first and second consecutive ET steps, respectively.

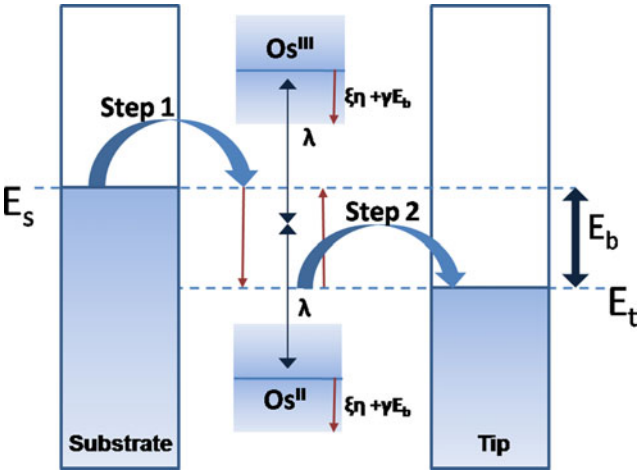

Fig. 1 Schematic representation of the two-step ET with partial vibration relaxation through the Os redox complex. Adapted from ref. [19] and ref. [36]

The charge state of the redox molecules can be precisely controlled by the electrochemical potential relative to a reference electrode (overpotential). Thus, the population of Os(II) and Os(III) species and the anions compensating charge at the surface as well as the change in solvation define the electronic level position of the redox bridge molecule as a function of the substrate electrode overpotential η. The total enhanced tunneling current is thus given by [15]

$$I_{\mathrm{tunn}} = \frac{1}{2}e\kappa\rho.(eE_{\mathrm{bias}})\frac{\varpi}{2\pi}exp\left(-\frac{\lambda + eE_{\mathrm{bias}}}{4k_BT}\right).\left[\cosh\left[\left(\frac{(^1/_2 - \gamma)eE_{\mathrm{bias}} - e\xi\eta}{2k_BT}\right)\right]\right]^{-1} \tag{7}$$

Notice that the local potential at the redox site in the nano-gap will be affected not only by the overpotential, η, but also by the tip to substrate bias potential, E_{bias}. Tuning the electrochemical potential relative to a reference electrode outside the nano-gap (overpotential, η) results in a change in the charge state of the osmium molecules, i.e., the population of Os(II) and Os(III) species, anions compensating charge at the surface and solvation energy. In the electrochemical EC-STS experiment, the tunneling current depends on the overpotential at fixed bias voltage with a maximum at E_{max} due to the variation of the activation Gibbs free energy, particularly by variation of the concentration of the oxidized and reduced states of the redox molecule. The position of the maximum depends on the local potential, i.e., the two parameters ξ and γ for each gating curve and is predicted by the equation [36]

$$E_{\mathrm{max}} = E^0 + (^1/_2 - \gamma)\frac{E_{\mathrm{bias}}}{\xi} \tag{8}$$

With the peak width given by

$$W = k_BT\lambda\sqrt{\frac{2\pi}{2\,k_BT\lambda + (eE_{\mathrm{bias}})^2}} \tag{9}$$

After the maximum the ET switches from the first step via Os(III) reduction to the second step via Os(II) oxidation, and it is not caused by the inverted region as in the Marcus theory [35].

Experimental

Materials

Diazonium salts of 2,3,5,6-tetrafluoro benzoic acid and of 4-aminobenzoic acid (preparation reported elsewhere) [38], C_3, C_6, C_8, C_{11}, and C_{16} mercapto alkanoic acids, 1-ethyl-3-(3-dimethylaminipropyl)-carbodiimide (EDC), *N*-hydroxysuccinimide (NHS), *N*-2-hydroxyethylpiperazine-*N*′-2-ethanesulfonic acid (HEPES), pH = 7.3, potassium perchlorate were used as received (Sigma-Aldrich) without further purification. The complex $Os[(bpy)_2(PyCH_2NH_2)Cl]PF_6$ has been synthesized as previously reported [23, 24].

Preparation of the gold surfaces

Two strategies have been employed to derivatize the gold substrate with the molecules represented in Fig. 2: self-assembled-monolayer of different alkanethiols in the case of Au-S bonds and the electrochemical modification using diazonium salts in the cases of Au-C bonds. Au on glass films (Arrandee®) were flame-annealed using hydrogen flame prior to use, in order to obtain extended plane terraces exposing (111) crystalline faces. Herringbone reconstruction was observed in air STM.

The diazonium technique to form Au-C bonds has been described elsewhere [25]. In brief, the benzoic acid and 2,3,5,6-tetrafluoro-benzoic acid were attached to gold surface by electro-reduction in a 5 mM solution of their corresponding diazonium salts (preparation reported elsewhere) [38] by chronoamperometry at 0.32 V vs. SCE for 5 min with 0.1 M tetrabutylammonium tetrafluoroborate in acetonitrile. The three-step gold substrate functionalization with alkanethiol was realized as described elsewhere for the Au-S system [23]. Au substrates were immersed in the respective mercaptane (10 mM) in ethanol solution for 24 h. The modified Au surfaces were then incubated in EDC (40 mM)-NHS (10 mM) solution in water for 1 h, and finally exposed to $[Os(bipy)_2Cl(py\text{-}CH_2\text{-}NH_2)]PF_6$ (0.5 mM) in 50 mM HEPES buffer solution (pH = 7.3) overnight.

Electrochemical experiments

Electrochemical measurements were carried out with an Autolab V 30 system (Eco Chemie, Utrecht, The Netherlands) controlled by a General Purpose Electrochemical Software (GPES) or FRA Software. This potentiostat is equipped with 750-kHz bandwidth ADC750 fast sampling module and scangen analog sweep module. All experiments were carried out at room temperature (20 ± 2 °C). Cyclic voltammetry experiments were performed in a purpose-built, three-electrode Teflon cell, with an electrode exposed area of approximately 0.28 cm^2 delimited by an inert "o" ring. A Pt counter electrode and an Ag/AgCl, 3 M KCl reference electrode were employed, and potentials herein are reported with respect to this reference.

Electrochemical impedance spectroscopy experiments implemented a frequency response analyzer (FRA 2) and excitation frequency ranged between 10^6 and 1 Hz. The amplitude of the excitation signals was 10 mV. The electron transfer kinetic measurements were carried out with spherical gold working electrodes prepared by melting the end of a 150-μm diameter gold wire in a flame to form a sphere of approximately 400 μm in diameter. The low values for the cell time constants of these electrodes (Table 1), needed to measure fast kinetics, are the result of a small electrode size (small double layer capacitance) and low uncompensated resistance in highly concentrated electrolyte. For the slowest systems (MHDA and MUA), a gold wire of larger diameter (0.5 mm) has been used.

STM

A Scanning Probe Microscope AFM-STM 5500 (Agilent Technologies®) with four-electrode bipotentiostat for the independent control of substrate and tip potentials with respect to the reference electrode in the electrolyte was used. Picoview 1.14.4 software was used for all the study. Pt-Ir (80–20) etched tips and Pt-Ir (80–20) isolated tips (<10 pA leak current) were purchased from Agilent Technologies® for air and electrochemical STM imaging, respectively. The custom-made three-electrode PTFE cell was used with a Pt wire as counter electrode and a Ag/AgCl wire as quasi-reference electrode. $NaClO_4$ (0.1 M) was used as electrolyte.

Electrochemical STM spectroscopy

Electrochemical scanning tunneling spectroscopy was performed using the following procedure as shown in Fig. 3: the tip was approached to the surface until a typical feedback current of 0.5 nA was obtained at fixed bias potential. To check the stability of the system, the tip was placed over a flat gold (111) terrace and the feedback loop was turned off. A stable set up shows no significant variations in tunneling current over at least 10 s. Once the stability is achieved the experiment is started. The feedback loop is turned off again and a current-potential curve is recorded at the same time between 0.1 and 0.45 V vs. Ag/AgCl using a sweep rate of 500 mV s^{-1}. If the tip is far from an Os redox center the electrochemical response

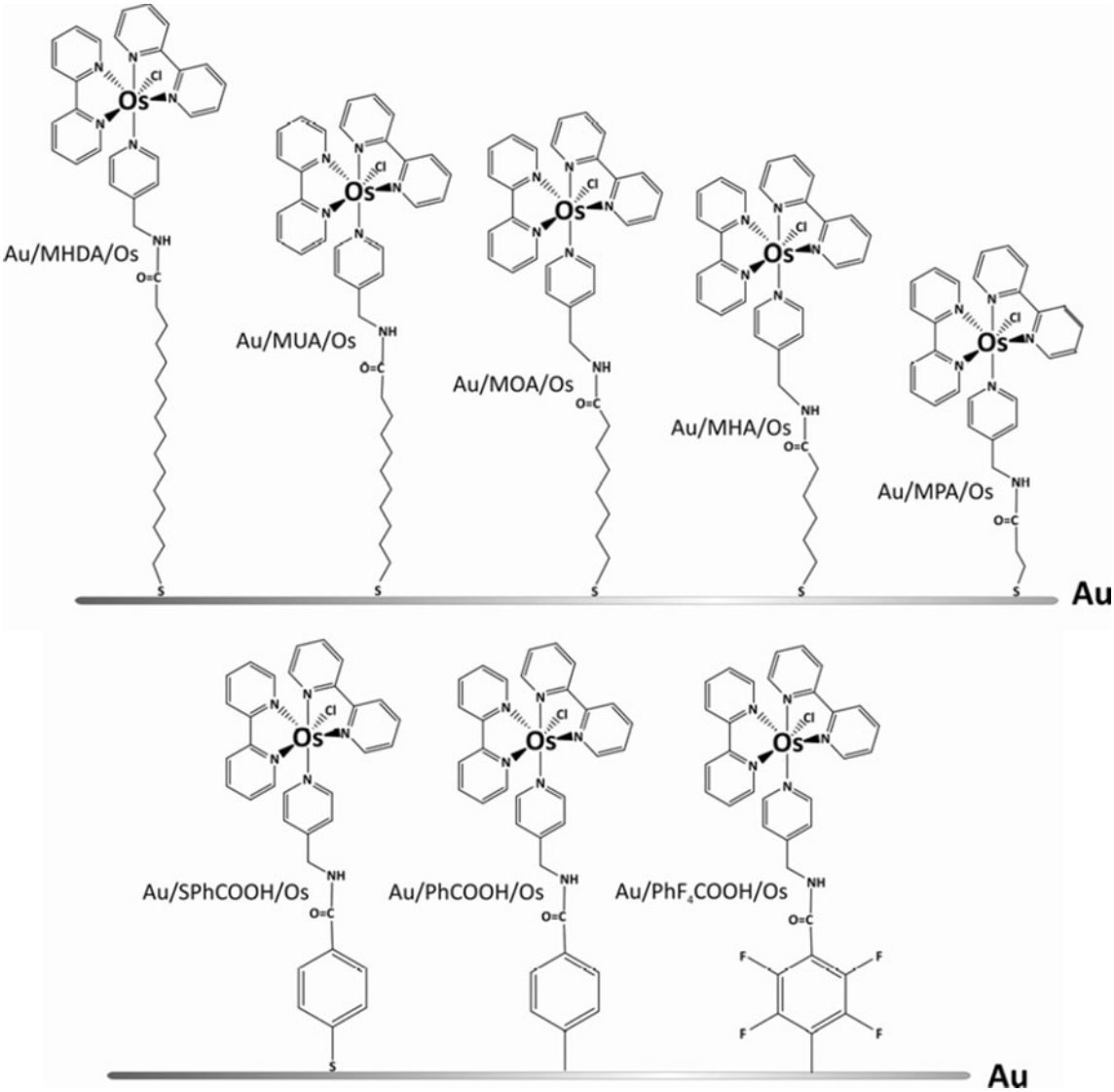

Fig. 2 Molecular structures of the different self-assembled monolayers functionalized with osmium complexes tethered to the gold surface from the left to the right: C_{16} (MHDA), C_{11} (MUA), C_8 (MOA), C_6 (MHA), and C_3 (MPA) mercapto alkanoic acids, 4-mercaptobenzoic acid (SPhCOOH), 4-aminobenzoic acid (Au/PhCOOH), and 2,3,5,6-tetrafluoro benzoic acid(Au/PhF_4COOH)

Table 1 Geometrical (length *d*) and electrochemical (formal potential ($E^{0\prime}$), peak separation (ΔE_p), charge (Q), surface coverage (Γ_{Os}), full width at half maximum (FWHM), electrode capacitance (C_{ads}), electrochemical rate constant (k^0_{ET}), cell time constant (R_SC_{dl})) properties of the tethered osmium complexes on gold

	MHDA/Os	MUA/Os	MOA/Os	MHA/Os	MPA/Os	SPhCOOH/Os	PhCOOH/Os	PhF_4COOH/Os
d/A	29.2	22.7	17.8	16.2	12.3	13.8	11.6	11.6
$E^{0\prime}/V$	0.28	0.28	0.30	0.28	0.30	0.30	0.30	0.32
$\Delta E_p/V$	0.03	0.01	0.02	0.02	0.01	0.03	0.06	0.02
Q/μC cm^{-2}	4.4	3.9	3.4	2.9	3.2	0.6	10	7.9
$\Gamma_{Os}/\times 10^{-10}$ lmol cm^{-2}	0.46	0.40	0.35	0.30	0.33	0.07	1.04	0.82
FWHM/V	0.15	0.14	0.13	0.13	0.13	0.14	0.16	0.11
k^0_{ET}/s^{-1}	13	1.9×10^3	1.3×10^4	2.5×10^4	2.1×10^5	1.9×10^5	1.4×10^5	3.0×10^5
$C_{ads}/\times 10^{-6}$ F	1.3	0.8	0.23	0.1	0.2	0.02	0.4	0.4
R_SC_{dl}/s	8×10^{-6}	9×10^{-6}	8×10^{-9}	1×10^{-8}	1×10^{-8}	8×10^{-9}	1×10^{-8}	9×10^{-9}

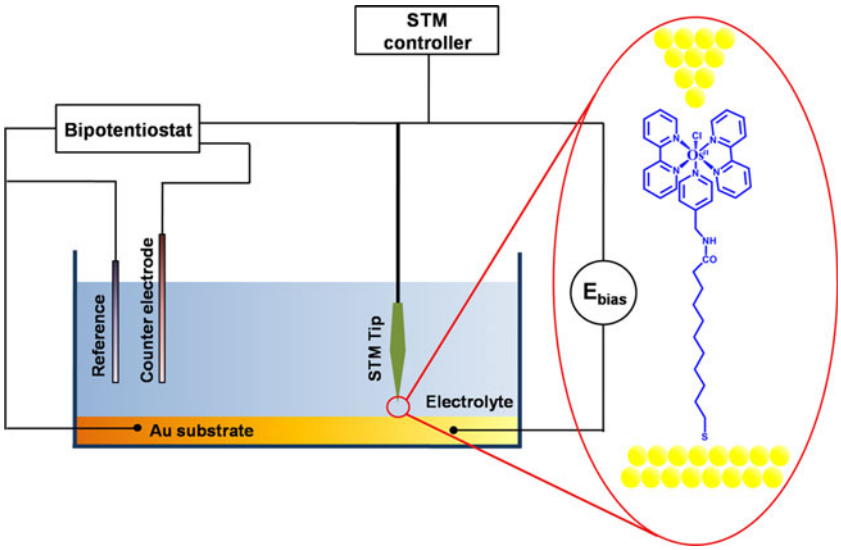

Fig. 3 Experimental set up for the EC-STS. Electrochemical scanning tunneling spectroscopy experiment. Adapted from reference [35]

gives no amplification feature. If the tip is close enough the typical amplification curve is obtained.

Results and discussion

STM imaging

A STM image of the MUA thiolated preferentially oriented Au(111) surface is depicted in Fig. 4a and shows well-defined terraces separated by monoatomic steps with the characteristic holes due to vacancy islands produced during alkane thiol adsorption [39].The inset in Fig. 4a shows a high-resolution image of a terrace with a $\sqrt{3} \times \sqrt{3}$ R30° lattice characteristic of adsorbed long alkanethiol ordered structures in good agreement to previous reports for MUA SAMs [40]. Figure 4b was taken in air after post-functionalization of the thiolated surface. Figure 4c shows similar osmium molecules on Au(111) immersed in the aqueous electrolyte at open circuit potential. Unlike the MUA thiol regular pattern, a disordered monolayer of the osmium complex is apparent from the bright spots with an average height of 0.8 nm in good agreement with the

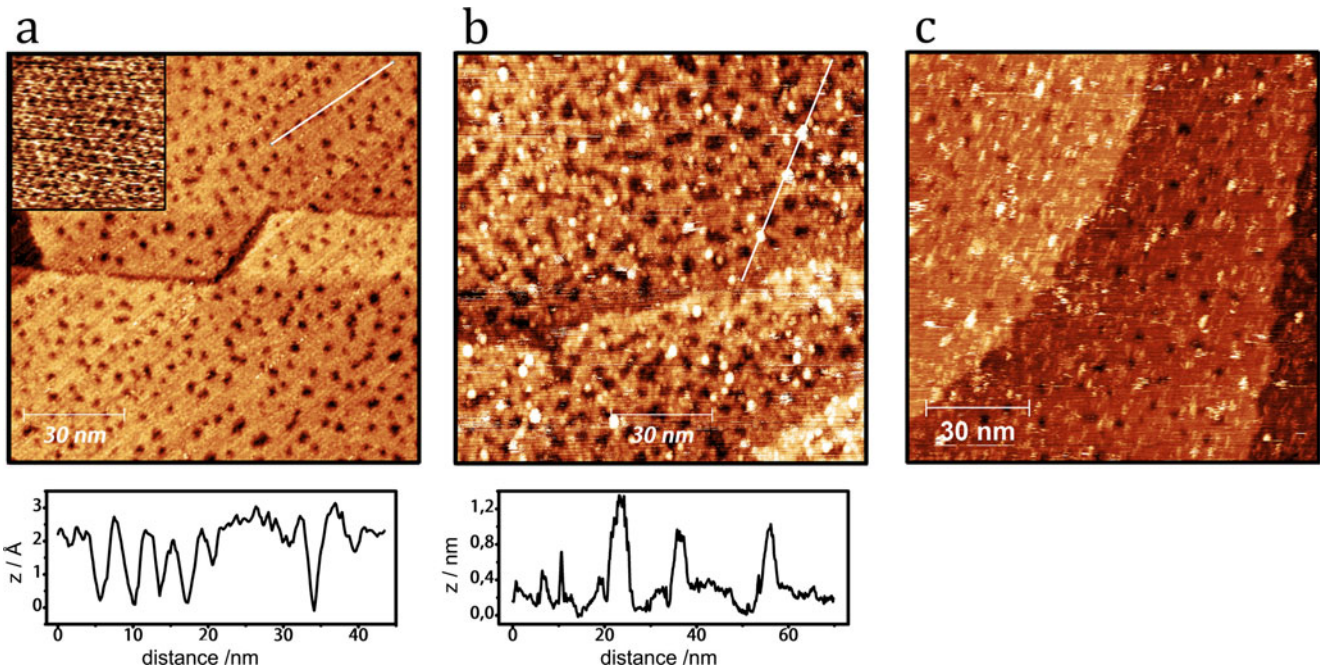

Fig. 4 **a** Air-STM of Au/MUA, *inset*: 8 × 8 nm high-resolution image. E_{bias} = 0.1 V, i_{tunn} = 1 nA. **b** Air-STM of Au/MUA/Os. E_{bias} = 1 V, i_{tunn} = 40 pA and the respective line profiles. **c** EC-STM of Au/MUA/Os in 0.1 M $NaClO_4$. E_{sample} = 0.25 V, E_{tip} = 0.75 V, and i_{tunn} = 0.3 nA

osmium complex size as calculated by DFT [41]. While the adsorbed thiol molecules are 0.5 nm apart and exhibit a tilt angle of 30°, the post-functionalization reaction is limited by the excluded volume of the osmium complex which is self-contained in an imaginary 0.62-nm diameter cylinder, thus yielding a maximum coverage of osmium for a closed packed structure of 1.3×10^{-10} mol cm^{-2} These results are similar to other osmium complexes in self-assembled monolayers [14, 23]. The bright spots in Fig. 4b correspond to the molecular size of the osmium complex though that the tunneling image was taken in the reduced Os(II) state off resonance.

ET in electrochemical experiments

The Os complex-modified Au electrodes were characterized by cyclic voltammetry and the surface concentration of redox molecules, Γ_{Os}, were calculated from integration of the cyclic voltammetry after subtraction of the double-layer charging current for the one electron Os(III)/Os(II) redox reaction. Figure 5 shows the monolayer voltammetry for MUA linker at different potential scan rates as predicted by Eq. (1) with a linear potential dependence on scan rate characteristic of surface redox species with fast electron transfer kinetics as described in our previous communications [26, 28].The full width at half height (FWHM) was in all cases larger than the ideal 90 mV for one electron Os(III)/Os(II) redox system due to repulsive interactions and counter ion and solvent effects. Table 1 compiles the linker length, the formal redox potential, peak separation, FWHM, redox charge, and surface redox concentration for $d = r - r_0$ (Eq. 3) ranging from 1.2 to 2.9 nm.

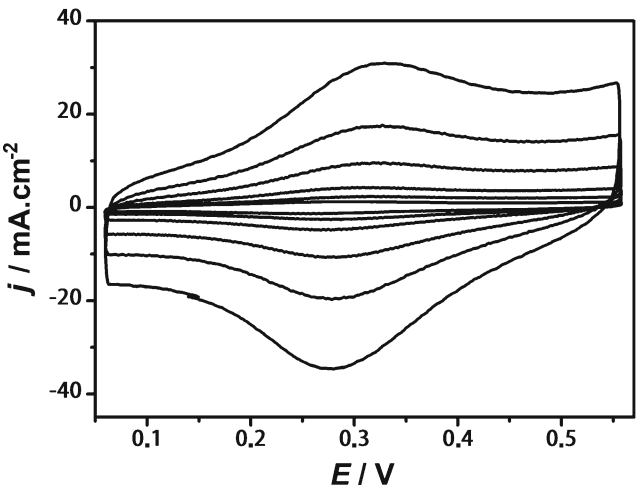

Fig. 5 Cyclic voltammetry of Au/MUA/Os in 0.1 M $NaClO_4$ at different scan rates: 0.05, 0.10, 0.20, 0.50, 1.0, and 2.0 V s^{-1}. $\Gamma_{Os} = 0.7 \times 10^{-10}$ mol cm^{-2} in the STM cell

It should be noticed that the surface coverage of redox groups from the STM image, i.e., 1.6×10^{-12} mol cm^{-2} is much less than that obtained from the integrated charge from low scan rate CV, i.e., 7×10^{-11} mol cm^{-2}. Since the tunneling image was taken off resonance, the bright spots in Fig. 4b probably represent only a fraction of the total osmium molecules self-assembled at the surface.

As can be seen from Table 1, the redox potential values range from 0.28 to 0.32 V vs. Ag/AgCl; 1 M KCl reference electrode as compared to the free soluble complex, 0.26 V. The difference is due to charge regulation at the surface by electrostatic effects [27].

The osmium complex studied in the present work shows a very fast ET kinetics, i.e., $k_{ET}{}^0 > 10^6$ s^{-1} similar to related osmium systems, i.e., $[Os(bpy)_2(p2p)Cl](PF_6)$ in $NaClO_4$ on Pt microelectrode, $k_{ET}{}^0 = 3 \times 10^5$ s^{-1} reported by Forster and Faulkner [34] or $Os(bpy)_2ClPy(CH_2)Py$ studied by Amatore et al. with $k_{ET}{}^0 = 4 \times 10^6$ s^{-1} by microelectrode ultrafast cyclic voltammetry [42].

A limitation to measure fast electrode kinetics is the cell time constant, i.e., the uncompensated resistance and the double-layer capacitance. In order to circumvent this drawback, we have measured kinetic constants for all systems depicted in Fig. 2 by the method proposed by Creager et al. [43, 44]. In this case, electrochemical impedance spectroscopy was employed and impedance spectra ($Z_{Re} + jZ_{Im}$ vs. f) were measured at different potentials. These potentials were chosen to be in a window centered at the formal potential ($E^{0\prime}$) of the redox couple (generally, between 0 and 0.5 V). At each potential, the impedance spectra were obtained at 25 different frequencies ranging between 10^6 and 1 Hz. From these spectra, the cell impedance was measured at each potential and each frequency and the variation of the cell admittance (Y) was analyzed as a function of potential for every frequency. This way, the cell admittance at the formal potential (Y_{peak}) and away from it (Y_{bkg}) were obtained and the ratio (Y_{peak}/Y_{bkg}) was plotted vs. log (f). The electron transfer kinetic constants were derived from these plots using the Randles equivalent circuit to model the electrochemical cell and fit the experimental data [43]

$$\frac{Y_{peak}}{Y_{bkg}} = \sqrt{\frac{\left(1+\frac{C_{redox}}{C_{dl}}\right)^2 + \frac{f^2}{4\left(k_{ET}^0\right)^2}}{1+\frac{f^2}{4\left(k_{ET}^0\right)^2}}} \tag{10}$$

with the electroactive film capacitance C_{redox} given by Eq. (1), C_{dl} the double layer capacitance and the standard electron transfer kinetic constant $k_{ET}{}^0$ given by Eq. (3) as fitting parameters and f is the frequency. Figure 6 shows the normalized results obtained according to Eq. (11) in order to facilitate

comparison between all systems and the parameters resulting from the fitting are summarized in Table 1. Furthermore, the cell time constants were calculated from R_S and C_{dl} values obtained from the cell impedance real and imaginary parts, respectively, measured at high frequency (details in Table 1)

$$\alpha = \frac{\left[Y_{peak} Y_{bkg} - 1\right]}{\left[\left(Y_{peak}/Y_{bkg}\right)_{max} - 1\right]} \quad (11)$$

Figure 6 shows the large effect on the frequency at which $\alpha = 0.5$ depending on the tether length. It should be noticed that for some systems, the fitting quality is poor probably due to a distribution of kinetic constants as suggested by Creager for similar *N*-(mercaptopentadecyl)ferrocenecarboxamide [43].

As the linker length decreases, α drops at higher frequencies since the ET kinetic constant increases, and the value of k_{ET}^0 obtained by Creager's method are plotted in Fig. 7 as a function of linker distance. A linear dependence with $\beta = 0.53$ Å^{-1} consistent with thought bond tunneling has been observed [45].

Electrochemical tunneling spectroscopy (EC-STS)

Electron transfer has also been studied in the asymmetric tunneling junction between the osmium bipyridine-pyridine complex tethered to a self-assembled alkanethiol on Au(111) surface and a Pt-Ir STM tip immersed in the aqueous electrolyte under an electrochemical environment (see Fig. 1).

In the electrochemical environment, the potential of both electrodes, Au substrate and tip in the nano-gap are controlled independently by the bipotentiostat with respect to a common reference electrode immersed in the electrolyte. In this

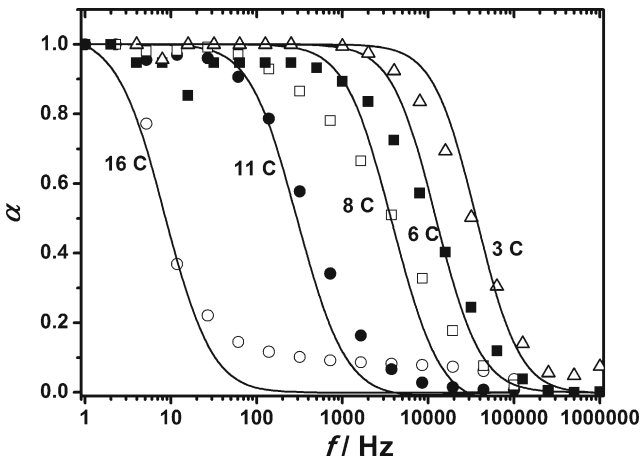

Fig. 6 Variation of α with excitation frequency in the Creager's method to estimate fast electron transfer rates

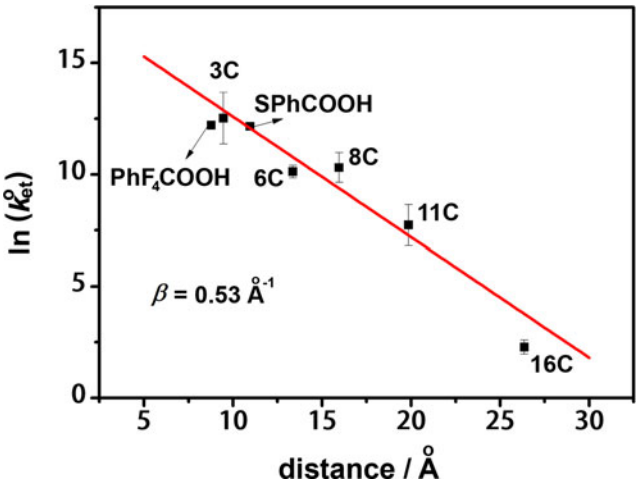

Fig. 7 Variation of the kinetic constant for electronic transfer as a function of the distance between Au and the redox osmium complex

experiment, the tip was approached at the tip current set point, typically 0.5 nA in the Os(II) state with the Au electrode at open circuit potential (off resonance). Then the feedback loop was disabled and the substrate electrode potential, E_S, was swept from the fully reduced Os(II) to the fully oxidized Os(III) state in the $E_s - E_{ref}$ potential window −0.25 to 0.25 V at 0.5 V s^{-1} while keeping the tip-sample bias potential, E_{bias}, constant. Negligible thermal drift on the time scale of the potential sweep experiment is needed so that the stability of the junction geometry is achieved by fast scan rate of 0.5 V s^{-1} and also Faradaic spurious tip currents during measurements are minimized by well-insulated tip (see Fig. 3).

Electron transfer in the asymmetric tunneling junction between the Au(111) substrate with the osmium bipyridine-pyridine monolayer and a Pt-Ir STM tip in aqueous electrolyte results in tunneling currents depicted in Fig. 8 for single scans. The tunneling current-overpotential curves for different E_{bias} show a maximum at $E_s = E_{peak}$ at constant E_{bias} which corresponds to half-oxidized and half-reduced osmium complex. At the extreme potentials, the set point current, I_0, due to direct (off resonance) tunneling is observed with no significant change of the molecular junction upon potential induced nano-gap structure and the tip to substrate distance does not change during a complete oxidation-reduction cycle in the 1 s time scale at 0.5 V s^{-1}.

From geometric considerations of the Au sample/molecule/tip nano-gap in the electrochemical environment and the very low conductance (I_0/E_{bias}), i.e., 1–4 nS in these experiments, it is expected that a few tethered osmium molecules or even single molecule events to occur. Thus, a stochastic exploration of molecules is performed, typically once every ten scans results in tunneling current amplification. Notice the fluctuations or noise in the single scan experimental curves shown in Fig. 8; this is ascribed to many fluctuations in the solvent shell

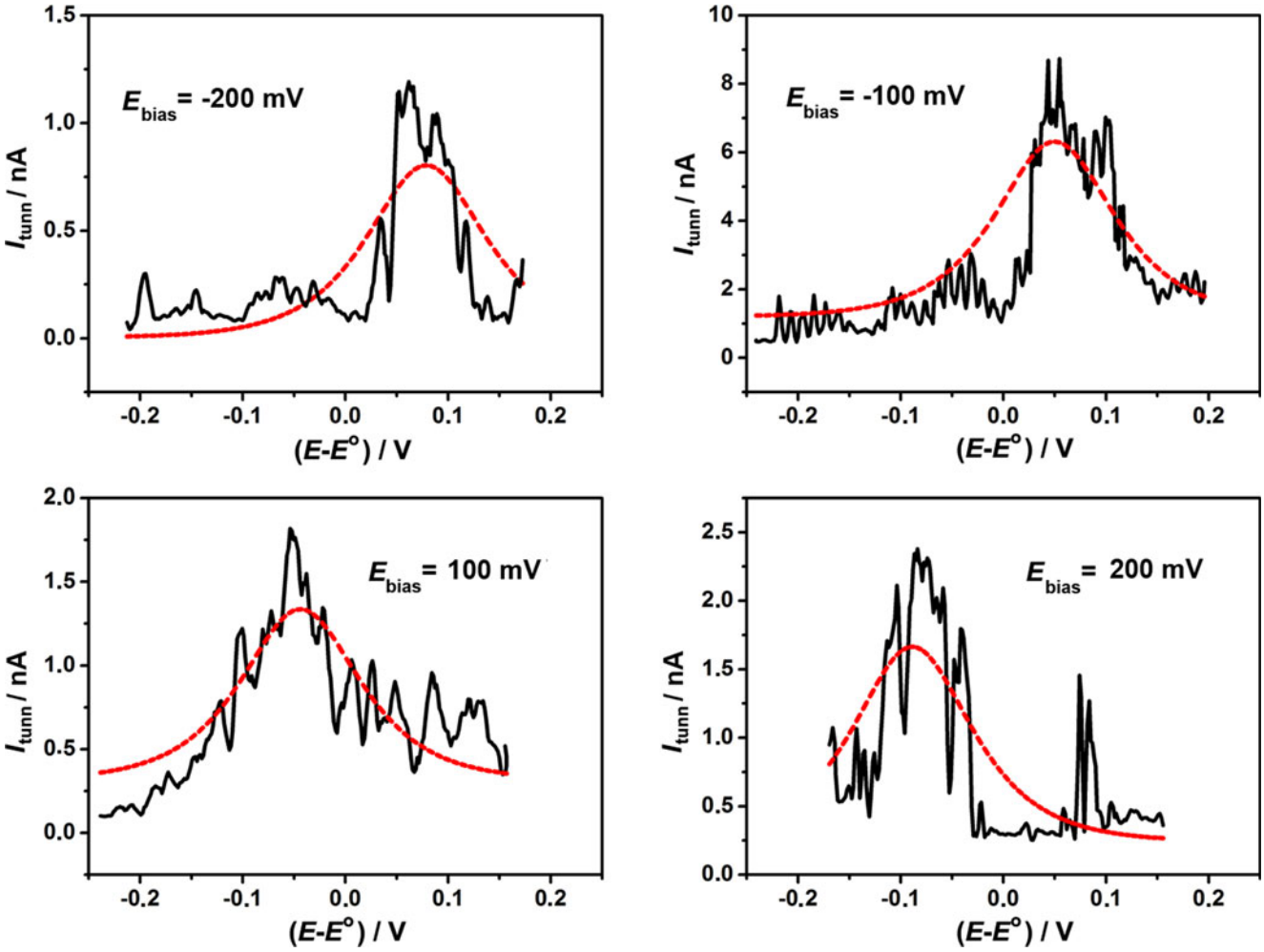

Fig. 8 Single experiment plot of i_{tunn} vs. $(E - E^0)$ for different E_{bias}. Au/MUA/Os in 0.1 M $NaClO_4$, E_s sweep rate 0.5 V s^{-1}. *Red curve* best fits to Eq. 12

around the Os center in the nano-gap during the time scale of the oxidation of Os(II) to Os(III), typically 1 s and to other sources of noise in the nano-gap.

In each case, we fitted the experimental tunneling current (i_{tunn}) vs. overpotential ($\eta = E_s - E^0$) curves to Eq. (7), using

$$i_{tunn} = i_0 + A\left[\exp\frac{\left[(0.5-\gamma)\times 1.602\times 10^{-19}E_{bias} - \left(1.602\times 10^{-19}\xi\eta\right)\right]}{8.225\times 10^{-21}} + \exp - \frac{\left[(0.5-\gamma)\times 1.602\times 10^{-19}E_{bias} - \left(1.602\times 10^{-19}\xi\eta\right)\right]}{8.225\times 10^{-21}}\right]^{-1} \quad (12)$$

with the corresponding value of E_{bias} for $-0.25 \le \eta \le 0.25$ V, i_0 the set point tunneling current, and

$$A = \frac{1}{2}e\kappa\rho(eE_{bias})\frac{\omega_{eff}}{2\pi}\exp\left[-\frac{\lambda + eE_{bias}}{4k_BT}\right] \quad (13)$$

The parameters ξ and γ were let free during the fitting process with the restrictions $0.5 < \gamma < 1$ and $0 \le \xi \le 1$.

Best fit values were obtained for $\xi = 0.9$–1 and $\gamma = 0.85$–1 and E_{peak} values vary linearly with E_{bias} as predicted by Eq. (8) and shown in Fig. 9.

From inspection of Eq. (9) for small E_{bias}, $((eE_{bias})^2 << 2k_BT\lambda)$, *the full width at half maximum (FWHM) of the curves in Fig. 7 is given by* $W = \sqrt{\pi\, k_B T\lambda}$. Values of FWHM in Fig. 7 are between 0.09 and 0.14 V which corresponds to a reorganization energy for the osmium molecule in the nano-gap of 0.11 to 0.24 eV, in agreement with previous reports for osmium complexes in similar experiments [22].

In the electrochemical experiments, the electron transfer rate, $k_{ET}{}^0$, varies from 13 to 10^5 s^{-1} for the same osmium molecule by decreasing the linkers distance from 2.9 to 1.3 nm due to tunneling from the electrode to the redox

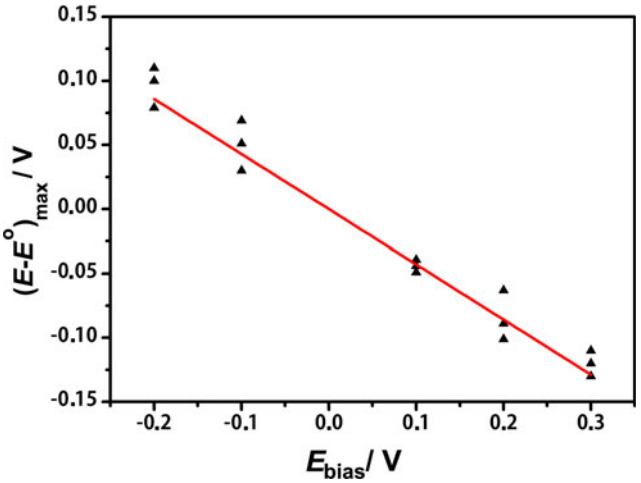

Fig. 9 Dependence of peak position with E_{bias} in Fig. 8

molecule. However, in EC-STS experiments the EC-gated enhanced tunneling current follows a sequential two-step mechanism which has been observed both for SPhCOOH/Os (1.4-nm distance) reported in a previous publication [23] and for MUA (2.3-nm distance) reported here. The time scale of a complete redox cycle, i.e., 1 s in the present case is much longer than the time constant for the electrochemical electron transfer, $\tau = (k_{ET}^{0})^{-1}$ both for short (10^{-5} s for SPhCOOH/Os) and long (10^{-3} s for MUA) linkers of the $Os[(bpy)_2(PyCH_2NH_2)Cl]^{+}$ complex. Therefore, the sequential two-step electron transfer from E_S to the redox osmium molecule and from this molecule to the tip electrode may take place many times during the reduction-oxidation cycle.

In the time scale of an Os(II) to Os(III) oxidation scan many fluctuations of the solvent around the osmium complex in the nano-gap can take place. Under strong electronic coupling between the redox molecule and both tip and substrate electrodes many electrons may be transferred in a single molecular redox cycle [36].

Conclusions

Electron transfer between Au electrodes and the redox molecule $Os[(bpy)_2(PyCH_2\ NH_2CO\text{-}]ClO_4$ tethered to Au surfaces via molecular linkers of different length (1.3 to 2.9 nm) has shown an exponential decay, k_{ET}^{0}, with $\beta = 0.53$ consistent with through bond tunneling to the redox center.

Electrochemical gating of single osmium molecules in the tunneling nano-gap between a Au(111) electrode and a Pt-Ir tip of a scanning tunneling microscope was achieved by independent control of the reference electrode potential in the electrolyte, $E_{ref} - E_s$, and the tip-substrate bias potential, E_{bias}.

Enhanced tunneling currents were observed at the redox potential of the Os(III)/Os(II) couple above the off resonance set point tunneling current for the totally reduced or totally oxidized redox complex.

A linear dependence of the overpotential at maximum current vs. the E_{bias} was recorded which corresponds to a sequential two-step electron transfer with partial vibration relaxation from the Au(111) substrate to the redox molecule in the nano-gap and from this redox complex to the Pt-Ir tip according to the model of Kuznetsov and Ulstrup [36].

The same behavior has been found for the osmium complex tethered with short and long linkers that may be due to the long time scale in the complete reduction-oxidation cycle in the electrochemical tunneling spectroscopy (EC-STS) experiment as compared to the time constants for electron transfer for all studied distances, k_{ET}^{0}.

Acknowledgments Financial support from the University of Buenos Aires, CONICET and ANPCyT is greatly acknowledged. We thank Prof. Mark Ratner for fruitful discussions on the mechanisms of ET.

References

1. Appleby AJ, Zagal JH (2011) Free energy relationships in electrochemistry: a history that started in 1935. J Solid State Electrochem 15(7–8):1811–1832
2. Bedioui F, Griveau S, Nyokong T, Appleby AJ, Caro CA, Gulppi M, Ochoa G, Zagal JH (2007) Tuning the redox properties of metalloporphyrin- and metallophthalocyanine-based molecular electrodes for the highest electrocatalytic activity in the oxidation of thiols. Phys Chem Chem Phys 9(26):3383–3396
3. Bingqian X, Tao NJ (2003) Measurement of single-molecule resistance by repeated formation of molecular junctions. Science 301(5637):1221–1223
4. Aviram A, Ratner MA (1974) Molecular rectifiers. Chem Phys Lett 29(2):277–283
5. Chidsey CED (1991) Free energy and temperature dependence of electron transfer at the metal-electrolyte interface. Science 251: 919–922
6. Marcus RA (1956) On the theory of oxidation-reduction reactions involving electron transfer. I J Chem Phys 24:966
7. Marcus RA (1957) On the theory of oxidation-reduction reactions involving electron transfer. II. Applications to data on the rates of isotopic exchange reactions. J Chem Phys 26:867
8. Marcus RA (1959) On the theory of eelectrochemical and chemical electron transfer processes. Can J Chem 37:155
9. Marcus RA (1965) On the theory of electron-transfer reactions. VI. Unified treatment for homogeneous and electrode reactions. J Chem Phys 43:679
10. Marcus RA (1993) Electron transfer reactions in chemistry: theory and experiment (Nobel lecture). Angew Chem Int Ed Engl 32(8): 1111–1121
11. Tao N (1996) Probing potential-tuned resonant tunneling through redox molecules with scanning tunneling microscopy. Phys Rev Lett 76:4066
12. Schmickler W, Tao NJ (1997) Measuring the inverted region of an electron transfer reaction with a scanning tunneling microscope. Electrochim Acta 42(18):2809–2815
13. Albrecht T, Guckian A, Ulstrup J, Vos JG (2005) Transistor-like behavior of transition metal complexes. Nano Lett 5:1451
14. Albrecht T, Moth-Poulsen K, Christensen JB, Guckian A, Bjornholm T, Vos JG, Ulstrup J (2006) In situ scanning tunnelling

spectroscopy of inorganic transition metal complexes. Faraday Discuss 131:265
15. Albrecht T, Moth-Poulsen K, Christensen JB, Guckian A, Bjørnholm T, Vos JG, Ulstrup J (2006) In situ scanning tunnelling spectroscopy of inorganic transition metal complexes. Faraday Discuss 131:265–279
16. Albretch T, Guckian A, Ulstrup J, Vos JG (2005) Transistor effects and in situ STM of redox molecules at room temperature. IEEE Trans Nanotechnol 4:430
17. Albretch T, Moth-Poulsen K, Christensen JB, Bjornholm T, Ulstrup J (2006) Scanning tunneling spectroscopy in an ionic liquid. J Am Chem Soc 128:6574
18. Li C, Mishchenko A, Li Z, Pobelov I, Wandlowski T, Li XQ, Würthner F, Bagrets A, Evers F (2008) Electrochemical gate-controlled electron transport of redox-active single perylene bisimide molecular junctions. J Phys Condens Matter 20(37)
19. Pobelov I, Zhihai L, Wandlowski TH (2009) Electrolyte gating in redox-active tunneling junctions an electrochemical STM approach. J Am Chem Soc 130:16045
20. Li Z, Liu Y, Mertens SFL, Pobelov IV, Wandlowski T (2010) From redox gating to quantized charging. J Am Chem Soc 132(23):8187–8193
21. Han B, Li Z, Li C, Pobelov I, Su G, Aguilar-Sanchez R, Wandlowski T (2009) From self-assembly to charge transport with single molecules—an electrochemical approach. Top Curr Chem 287
22. Zhou XS, Liu L, Fortgang P, Lefevre AS, Serra-Muns A, Raouafi N, Amatore C, Mao BW, Maisonhaute E, Schöllhorn B (2011) Do molecular conductances correlate with electrochemical rate constants? Experimental insights. J Am Chem Soc 133(19):7509–7516
23. Ricci AM, Calvo EJ, Martin S, Nichols RJ (2010) Electrochemical scanning tunneling spectroscopy of redox-active molecules bound by Au-C bonds. J Am Chem Soc 132(8):2494-+
24. Ricci A, Bonazzola C, Calvo EJ (2006) An FT-IRRAS study of nitrophenyl mono- and multilayers electro-deposited on gold by reduction of the diazonium salt. Phys Chem Chem Phys 8(37):4297–4299
25. Saby C, Ortiz B, Champagne GY, BÃ©langer D (1997) Electrochemical modification of glassy carbon electrode using aromatic diazonium salts. 1. Blocking effect of 4-nitrophenyl and 4-carboxyphenyl groups. Langmuir 13 (25):6805–6813
26. Ricci AM, Rolli C, Rothacher S, Baraldo L, Bonazzola C, Calvo EJ, Tognalli N, Fainstein A (2007) Electron transfer at Au surfaces modified by tethered osmium bipyridine-pyridine complexes. J Solid State Electrochem 11:1511–1520
27. Ricci AM, Tagliazucchi M, Calvo EJ (2012) Charge regulation in redox active monolayers embedded in proton exchanger surfaces. Phys Chem Chem Phys 14(28):9988–9995
28. Ricci AM, Tognalli N, de la Llave E, Vericat C, Mendez De Leo LP, Williams FJ, Scherlis D, Salvarezzac R, Calvo EJ (2011) Electrochemistry of os(2,2′-bpy)(2)ClPyCH2NHCOPh tethered to Au electrodes by S-Au and C-Au junctions. Phys Chem Chem Phys 13(12):5336–5345
29. Bard AJ, Faulkner LR (2001) Electrochemical methods, 2 edn. Wiley, New York
30. Gerischer H (1960) Z Phys Chem NF 26:223
31. W. Schmickler, Frank S. (2003) Quantum theory of electrochemical electron-transfer reactions. In: Calvo EJ (ed) Interfacial kinetics and mass transport, vol 2, Ch. 2. Encyclopedia of electrochemistry. Wiley VCH, Weinheim, pp 31–48
32. Nitzan A (2001) Electron transmission through molecules and molecular interfaces. Annu Rev Phys Chem 52:681
33. Nitzan A (2003) Electronic tunnel factors in molecular electron transfer and molecular conduction. In: Calvo EJ (ed) Interfacial kinetics and mass transport, vol 2. encyclopedia of electrochemistry. Wiley VCH, Weinheim, pp. 49–78
34. Miller CJ, Rubinstein I (1995) Physical electrochemistry. Marcel Dekker, New York
35. Zhang J, Kuznetsov AM, Medvedev IG, Chi Q, Albrecht T, Jensen PS, Ulstrup J (2008) Single-molecule electron transfer in electrochemical environments. Chem Rev 108:2737–2791
36. Kuznetsov A, Ulstrup J M (2000) Mechanisms of in situ scanning tunnelling microscopy of organized redox molecular assemblies. J Phys Chem A 104:11531
37. Zhang J, Chi Q, Kuznetsov A, Hansen AG M, Wackerbarth H, HEM C, JET A, Ulstrup J (2002) Electronic properties of functional biomolecules at metal/aqueous solution interfaces. J Phys Chem B 106:1131
38. Ricci AM, Mendez De Leo LP, Williams FJ, Calvo EJ (2012) Some evidence for the formation of an azo bond during the electroreduction of diazonium salts on Au substrates. ChemPhysChem 13(8):2119–2127
39. Vericat C, Vela ME, Salvarezza RC (2005) Self-assembled monolayers of alkanethiols on Au(111): surface structures, defects and dynamics. Phys Chem Chem Phys 7(18):3258–3268
40. Kakiuchi T, Iida M, Gon N, Hobara D, Imabayashi SI, Niki K (2001) Miscibility of adsorbed 1-undecanethiol and 11-mercaptoundecanoic acid species in binary self-assembled monolayers on Au(111). Langmuir 17(5):1599–1603
41. De La Llave E, Ricci A, Calvo EJ, Scherlis DA (2008) Binding between carbon and the Au(111) surface and what makes it different from the S-Au(111) bond. J Phys Chem C 112(45):17611–17617
42. Amatore C, Bouret Y, Maisonhaute E, Abruña HD, Goldsmith JI (2003) Electrochemistry within molecules using ultrafast cyclic voltammetry. C R Chim 6(1):99–115
43. Creager SE, Wooster TT (1998) A new way of using ac voltammetry to study redox kinetics in electroactive monolayers. Anal Chem 70(20):4257–4263
44. Creager SE, Yu CJ, Bamdad C, O' Connor S, MacLean T, Lam E, Chong Y, Olsen GT, Luo J, Gozin M, Kayyem JF (1999) Electron transfer at electrodes through conjugated "molecular wire" bridges. J Am Chem Soc 121:1059–1064
45. Finklea HO (2003) Electron transfer. In: JFR M, Rubinstein I (eds) Modified electrodes, vol 10. Encyclopedia of electrochemistry. Wley-VCH, Weinheim, pp. 625–650